# Aerodynamic performance investigation of a Rib Roughened Cooling Channel Flow with high blockage ratio.

by

L. CASARSA [(1)] and T. ARTS [(2)]

[(1)] Dipartimento di Energetica e Macchine, University of Udine, via delle Scienze 208, 33100 Udine, Italy; E-mail: casarsa.luca@spes.uniud.it

[(2)] von Karman Institute for Fluid Dynamics, Turbomachinery and Propulsion Department, 72, chaussée de Waterloo, B1640 Rhode Saint Genèse, Belgium ; E-mail: arts@vki.ac.be

## ABSTRACT

The present study deals with a detailed experimental investigation of the turbulent flow inside a rib-roughened turbine blade cooling channel. The main objective is to enhance the understanding and deepen the analysis of this complex flow field with the help of highly resolved Particle Image Velocimetry aerodynamic measurements. These measurements also constitute the necessary complement to the already reported wall heat transfer distributions. In this way, a wide and reliable data base is also made available for numerical code validation. In addition, a coherent structure eduction is performed by means of a wavelet approach in the symmetry plane of the channel. This analysis allows to draw additional conclusions about some of the measured turbulent structures.

The measurements are carried out at correct Reynolds number within a scaled up model of a stationary straight cooling channel, with turbulent promoters (ribs) installed on one wall. These ribs present a high blockage ratio (30 %) and are perpendicular to the "mean" flow direction.

A global three dimensional view of the velocity field is provided by applying the PIV technique in between two consecutive ribs along different and mutually perpendicular planes. The highly resolved data allow a very exhaustive description of a number of particular flow structures. The combined analysis of both aerodynamic and heat transfer results puts in evidence the role of the mean and fluctuating flow features in the heat transfer process.

The wavelet analysis allows the detection of coherent structures. These vortices are however only the footprints of more complicated structures which develop in all spatial directions. A statistical analysis provides valuable information on the flow topology. The existence of a significant peak in the distributions of the detected structure's core size and vorticity (or circulation) suggests the existence of a most probable vortex into the flow field. A conditional averaging is applied on the detected structures, phase-aligned with the preferred mode, leading to the definition of a typical eddy vorticity pattern.

## 1. INTRODUCTION

Nowadays, the need for high power and high efficiency gas turbine engines forces the designer to continuously increase the turbine inlet temperature (TIT). In recent military applications, the TIT could be as high as 2000 K, far above the melting temperature of the most advanced vane and blade materials. The efficiency of the blade cooling system is therefore strictly related to the safe operation of the engine and a complete understanding of the convection mechanisms resulting from the cooling techniques is mandatory. The present experimental contribution therefore focuses on the aerodynamic behaviour of a rib-roughened channel flow, as encountered in high pressure turbine vanes.

A number of experimental investigations about internal cooling channels with ribs are available in the open literature. Most of them are however only concerned with the heat transfer performance (Han, 1988, Han et al., 1992, Taslim, 1997). Detailed aerodynamic measurements were nevertheless performed by Schabacker et al. (1999) or Chanteloup and Boelcs (2001), among a few other authors. Numerical simulations of the velocity and heat transfer fields were proposed by Liou et al. (1993), Rigby (2000) and Sagaut (2000) who did one of the few DNS and LES computations available in literature on this configuration. The combination of aerodynamic and heat transfer measurements on the same channel configuration and with the same boundary conditions seldom appears, and very often the data are too scarce to provide a complete quantitative description of the flow field.

The aim of the present work is to fill this gap by providing detailed flow field measurements that, together with the corresponding wall heat transfer measurements, constitute a wide and reliable experimental data base on the aero-thermal performance of a rib-roughened cooling channel. The analysis of this data set will allow to improve the understanding of this complicated flow and might help in the selection or the development of an appropriate turbulence model for such a configuration.

The experiments are carried out on a scaled up model of a real cooling channel, maintaining geometrical and kinematic similarity conditions. Turbulence promoters (ribs) with a high blockage ratio are installed along one of the walls. The velocity field is measured by means of Particle Image Velocimetry (PIV) in between two consecutive ribs along mutually perpendicular planes. The interpretation of the PIV data provides an exhaustive description of the mean flow topology. The combined analysis of the aerodynamic results with the available wall heat transfer data allows to point out the role played by the mean flow features and by the velocity fluctuations in the heat transfer process.

The spatial resolution characterizing the PIV data gives access to the investigation of the Coherent Structures (CS) developing inside the flow field. The interest of the researcher for the CS is mainly dictated by the evidence that the CS play a crucial role in many phenomena of industrial interest such has turbulent mixing, aero-acoustics, drag reduction, heat transfer … etc. It should also be mentioned that, ultimately, the study of the CS can bring useful information to the understanding of the turbulent flow, but this is out of the scope of the present paper. So far, the authors did not find in the open literature any description of a similar configuration in terms of CS evolution except for the numerical investigation of Sagaut (2000) previously mentioned. A wavelet approach is used in the present work to educe the CS from the instantaneous flow fields measured in the channel symmetry plane. Unfortunately the use of uncorrelated flow images provided by the PIV system does not allow to follow the evolution of the detected structures in space and time. Nevertheless, it will be seen that useful information about the flow topology can still be obtained.

## 2. EXPERIMENTAL APPARATUS

### 2.1 Flow Configuration

The geometry of the test section used for this investigation is shown in Fig. 1. It represents a scaled up model of an internal cooling channel for gas turbine vanes, with a squared section of 100 × 100 mm$^2$ and a length of 2800 mm.

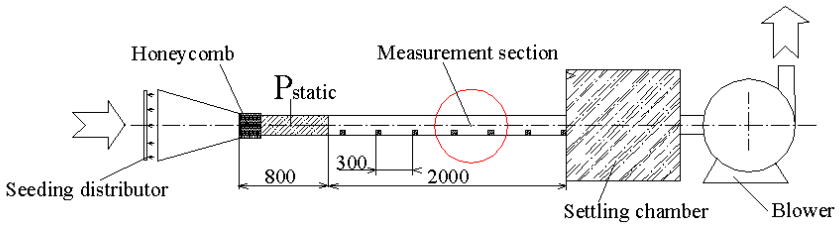


**Fig. 1: Schematic of the test section**

To ensure the necessary optical access for the PIV measurements, the measurement section is made of Plexiglas, while the entrance part is made of wood. Seven Plexiglas ribs are installed on one wall of the channel. They have a squared section of 30 × 30 mm$^2$, providing therefore a blockage ratio of 30%, and an angle of attack of 90 deg with respect to the mean flow direction. Their pitch-to-height ratio (p/h) is equal to 10. Air at atmospheric pressure and temperature is aspirated through the channel by means of a centrifugal blower. The flow rate is quantified by measuring the inlet velocity profile and the wall static pressure at the channel inlet. The velocity profile are measured at 8 hydraulic diameters downstream the test section entry. The velocity profiles are symmetric and turbulent but not completely developed. The boundary layer thickness is about 30 % of the hydraulic diameter. The mass flow is set in order to get an engine representative Reynolds number (40,000).

The flow field data are acquired in between the 4$^{th}$ and the 5$^{th}$ rib of the channel where, as checked, the mean flow is periodic. Six different measurement planes are considered (Fig. 2). Plane 1xy is the symmetry plane of the channel (Z/h=0), planes 2xy and 3xy are located respectively at 20 mm (Z/h=1) and 5 mm (Z/h=1.5) from the lateral wall. Plane 1xz is positioned at 1.5 mm (Y/h=0.05) from the ribbed wall, plane 2xz at half rib height (Y/h=0.5) and plane 3xz at 3 mm above the rib upper surface (Y/h=1.1).

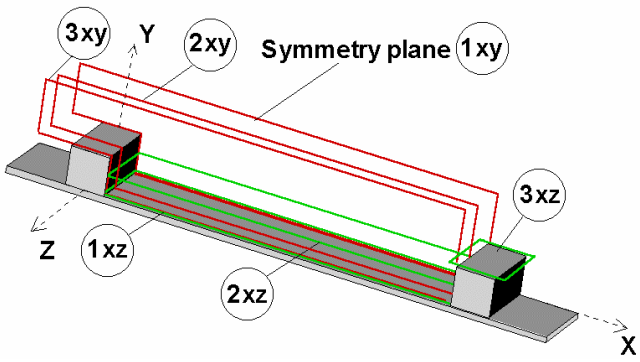


**Fig. 2: PIV measurements planes**

### 2.2 PIV Measurement Chain and Data Processing

The PIV set-up is made of a 2 cavities Nd-YAG laser, a CCD camera (1280 x 1024 pixels resolution) and a signal generator to synchronize them. The flow is seeded by small oil particles provided by a Laskin nozzle type seeding generator. The PIV images are processed using W.I.DI.M. (Window Displacement Iterative Multigrid), a software developed at VKI by Scarano and Riethmuller (1999). The uncertainty on the instantaneous velocity is estimated to be less than 2%, based on the Kline and Mc Clintock (1953) analysis,

The procedure proposed by Cramer (1955) and Riethmuller and Lourenco (1981) is used to determine the number of samples needed to ensure the convergence of the statistical quantities, such as mean and rms velocities. About 300 samples are found to be sufficient to yield a time-averaged flow field with a limited error on the mean velocity (<5%) and on its rms (<10%) within the complete measurement domain except for a small portion on top of the rib and in the core of the shear layer. Details about the PIV chain operating parameters, the processing of the PIV images and the statistical approach used to analyze the data are described by Casarsa et al. (2002).

## 3. PIV DATA DISCUSSION

Fig. 3 shows the time averaged velocity field in the symmetry plane (1xy).

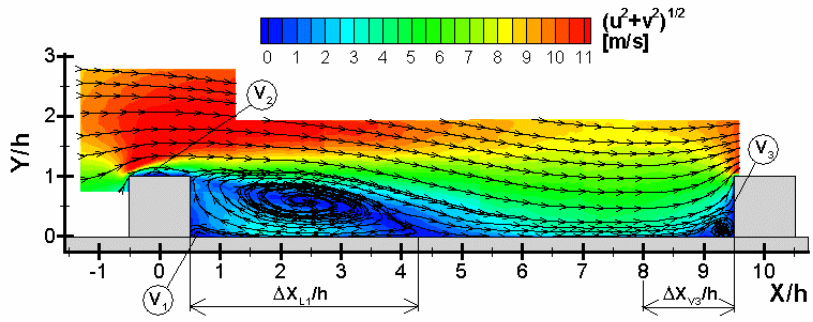


**Fig. 3: Time averaged velocity field in plane 1xy**

From the contour lines, it is clear how the obstacle, by reducing the available cross section, induces a strong acceleration of the flow. This behavior is confirmed by wall static pressure measurements (Casarsa et al., 2002). The sudden expansion downstream of the rib and the consequent flow separation leads to the generation of a strong shear layer associated to a wide recirculation region which, in the averaged flow fields, appears as an organized swirling flow structure. After the reattachment, the flow re-aligns with the bottom wall and a new boundary layer develops. The latter is accelerated by the free stream shear forces until it impinges on the next obstacle generating a second separated region in front of this rib ($V_3$, Fig. 3). Two other separated flow regions are identified in plane 1xy. The first one is located on top of the rib ($V_2$, Fig. 3) while the second one is a small corner vortex in the downstream bottom edge of the obstacle ($V_1$, Fig. 3), counter-rotating with respect to the main separation bubble. High spatial resolution measurements have been especially dedicated to the definition of the size and localization of structures $V_1$ and $V_3$ and are reported in a previous paper (Casarsa et al., 2002).

Fig. 4 shows the turbulence intensities (defined as the rms of the velocity fluctuations normalized by the bulk velocity $U_0 = 6.2$ m/s) along the streamwise and vertical directions in plane 1xy. The highest values are observed on top of the rib, at separation onset. Very close to the ribbed wall, the highest fluctuations are observed in a region centered on the mean reattachment point and in a small area in front of the rib (see also Fig. 11). The measurements clearly demonstrate the strong anisotropic character of the turbulent phenomena.

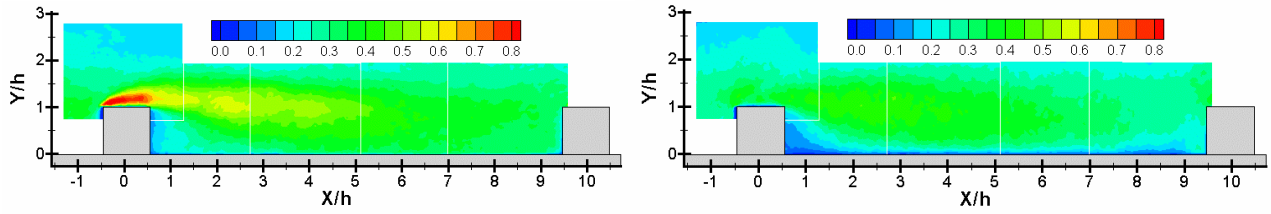


**Fig. 4: Turbulence intensity contour plots in the streamwise (left) and vertical (right) directions (plane 1xy)**

The contour plot of the Reynolds stresses in plane 1xy is given in Fig. 5, showing the strength of the separated shear layer. Significant negative values are reported in a small flow region above the top upstream corner of the rib. This behavior is due to the strong local acceleration. The flow is aligned along a preferential direction (about 35 deg),

showing correlated fluctuations in the streamwise and vertical velocity components (u'and v' are both either positive or negative or, in other words, the product of the instantaneous u'v' is always positive). If, in this area, the fluctuation in u' and v' would be computed along a reference system whose x axis is aligned with the mean flow direction, the resulting Reynolds stresses would be positive, as normally expected.

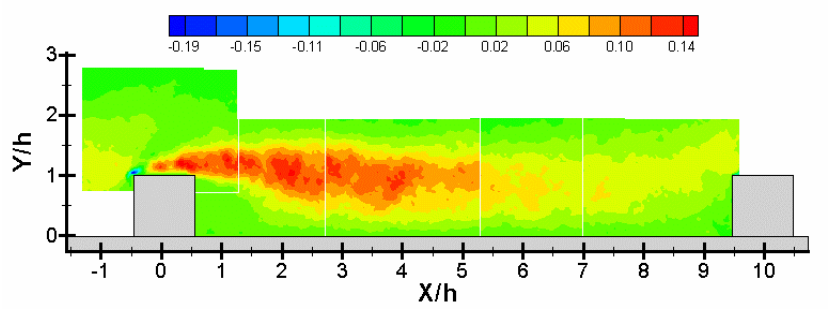


**Fig. 5: Reynolds stresses $-\left(\overline{u'v'}/U_0\right)$ in plane 1xy**

In plane 2xy, the flow behavior is mainly the same as in plane 1xy. The flow is generally slower and less turbulent because of the effect of the boundary layer on the channel side walls.

Fig. 6 shows the mean flow features in plane 1xz. The reattachment line $L_1$ is clearly visible. Near the lateral wall it exhibits a particular shape (Figs. 8 & 9), as already observed by Rau et al. (1998) for a similar configuration but a smaller blockage. This behavior has been explained by Casarsa et al. (2002), who propose a model based on the hypothesis of the side wall boundary layer deviation imposed by the rib.

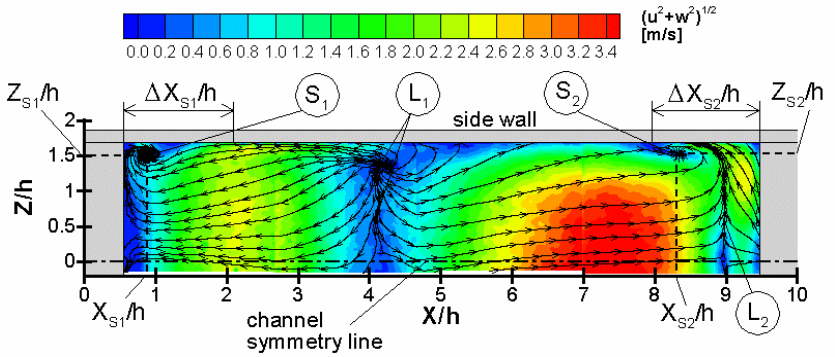


**Fig. 6: Time averaged velocity field in plane 1xz**

In plane 1xz, the separation line $L_2$ associated with the separation bubble $V_3$ seen in planes 1xy and 2xy is also put in evidence. Moreover, the entrained flow shows a transverse motion which acts towards the side walls in the rib vicinity and towards the channel centerline in the reattachment area. This behavior is consistent with earlier wall static pressure measurements. Finally, in the rib vicinity, the stream tracers spiral around two sinks, namely the mean structures $S_1$ and $S_2$. High values of spanwise turbulence intensity are found in the reattachment area and upstream of the rib (Fig. 7). The highest values are twice as large as those of the vertical fluctuations in plane 1xy, stressing again the anisotropic character of the turbulent phenomena.

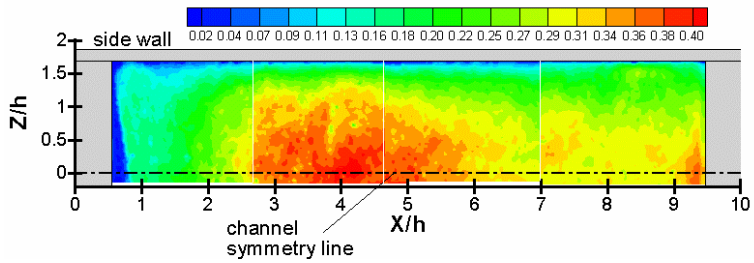


**Fig. 7 : Spanwise turbulence intensity in plane 1xz**

The transverse flow motion is not observed anymore in plane 2xz (Fig. 8). The separation bubble limit clearly appears from the stream tracers path. The structures $S_1$ and $S_2$ are still present at this height (0.5 h). Together with the structures $V_1$, $V_2$ and $V_3$ they sustain the separated three-dimensional region around the obstacle.

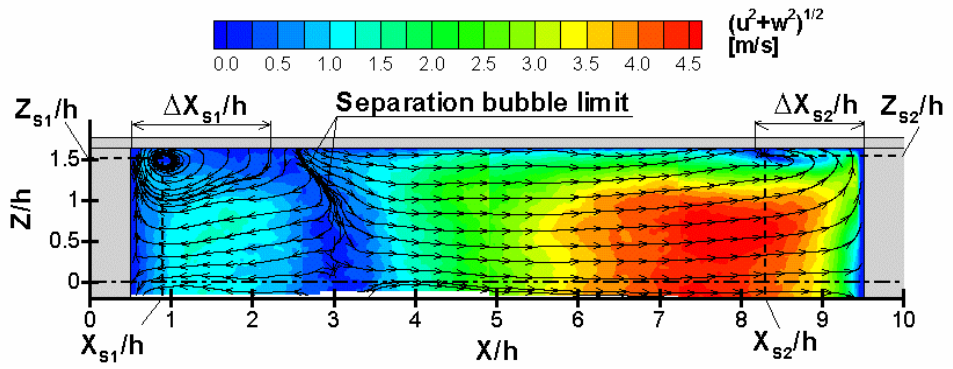


**Fig. 8 : Time averaged velocity field in plane 2xz**

Above the rib (plane 3xz), the flow is characterized by the separation bubble $V_2$, which grows moving from the channel centerline towards the lateral walls (Fig. 9). Looking at the corners between the rib edges and the side wall, the mean flow structures $S_1$ and $S_2$ still seem to be present. The contour plots of the turbulence intensities in plane 3xz (Fig. 10) clearly show how all the fluctuations are generated on top of the rib, inside the recirculation bubble $V_2$.

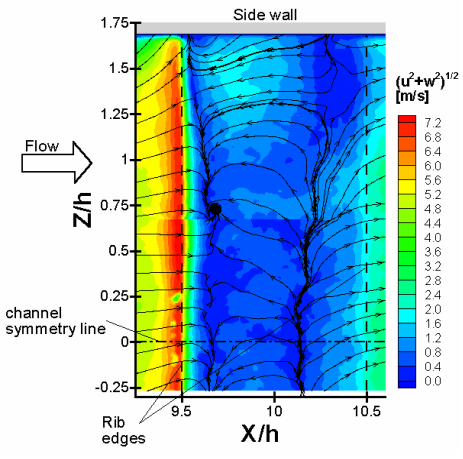


**Fig. 9: Time averaged velocity field I in plane 3xz**

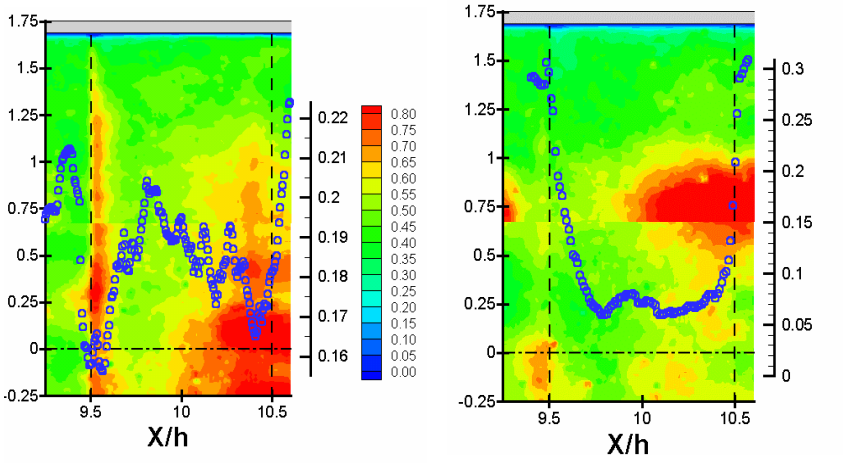


**Fig. 10: (left) Streamwise turbulence intensity contour plot, vertical turbulence intensity profile (plane qxy at Y/h=1.01); (right) spanwise turbulence intensity contour plot, vertical turbulence intensity profile (plane 2xy at Y/h=1.01)**

The description of the mean flow behavior given up to here confirms and extends with new information the flow model proposed by Rau et al. (1998). Information about the localization and dimensions of all the identified flow characteristics are provided by Casarsa et al. (2002).

Çakan (2000) carried out an exhaustive measurement campaign to determine the heat transfer distribution along the various walls and on the ribs of the same channel by means of Liquid Crystal Thermography. By combining the data from Çakan and the detailed PIV measurements presented in this work, it becomes possible to make some interesting observations on the aero-thermal flow behavior.

The profile of the enhancement factor ($Nu/Nu_{smooth\ channel}$) on the ribbed wall along the channel centerline is shown in Fig. 11. The profiles of the normal to the wall ($V_{rms}/U_0$) and streamwise ($U_{rms}/U_0$) velocity fluctuations extracted from the PIV measurements in the symmetry plane at Y/h=0.1 are presented on the same graph. This comparison shows how the heat transfer distribution appears to be more strongly affected by the velocity fluctuations normal to the wall, showing a clear correlation between maximum heat transfer and maximum $V_{rms}$ (regions located around the reattachment point (X/h≈4.5) and in front of the rib (X/h≈8.5)). The same behavior is extracted within plane 2xy (Fig. 12).

Similar data have been extracted from the planes 2xz and 3xz and compared with heat transfer data on the channel lateral wall (Figs. 13 & 14). In these locations, the heat transfer distribution maxima show a correlation with both the streamwise (U) and normal to the wall (W) components of the velocity fluctuations. This is clearer in Fig. 13,

where the data along the full inter-rib space are available. The same correlation is found in the region on top of the rib (Fig. 15). The highest level of heat transfer is found in the central part of the rib upper surface; it coincides with the maxima in streamwise and vertical fluctuations.

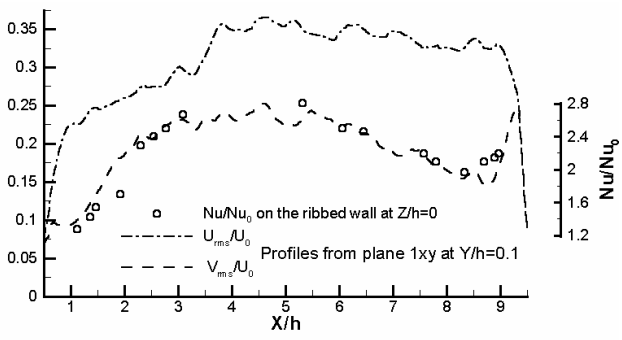


**Fig. 11: Near wall normal and streamwise velocity fluctuations and heat transfer enhancement factor on the bottom wall along the channel centerline (Z/h=0)**

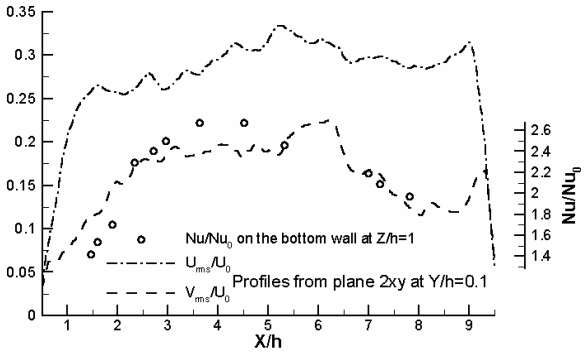


**Fig.12: Near wall normal and streamwise velocity fluctuations and heat transfer enhancement factor on the bottom wall (Z/h=1)**

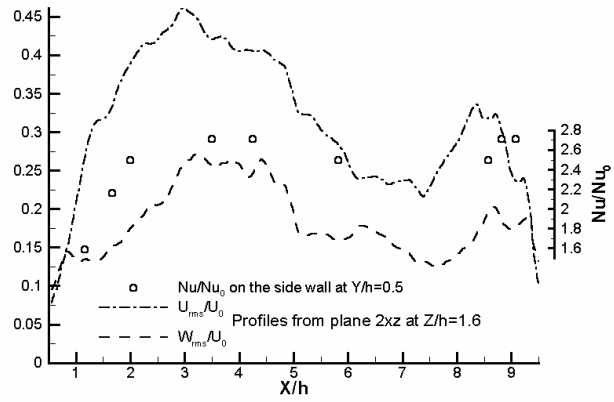


**Fig. 13 : Near wall normal and streamwise velocity fluctuations and enhancement factor distributions on the lateral wall (Y/h=0.5)**

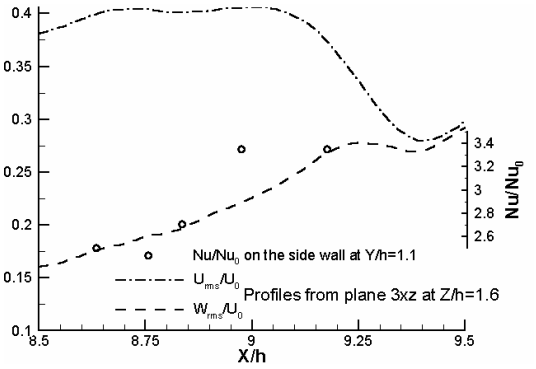


**Fig. 14 : Near wall normal and streamwise velocity fluctuations and enhancement factor distributions on the lateral wall (Y/h=1.1)**

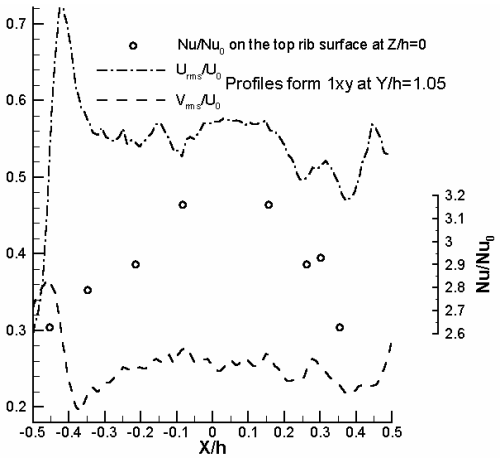


**Fig. 15 : Near wall normal and streamwise velocity fluctuations and enhancement factor in the region on top of the rib (Y/h=1.1)**

Further investigations are underway, based on a more detailed analysis of the present data, aiming to understand which are the most effective flow mechanisms in the development of the heat transfer field. This information, if available, might shed some light on the selection of the appropriate turbulence model. Indeed, the

simulation of this rib-roughened channel flow proved to be still a challenging task in modern CFD. It is experience of the present authors that the use of standard k-ε turbulence models does not lead to accurate predictions of both the flow and heat transfer fields. The use of more advanced modeling approaches, which consider the anisotropic character of the near wall velocity fluctuations, proved to be quite efficient for this kind of application, (Durbin ,1993 and Hermanson et al., 2001).

## 4. WAVELET ANALYSIS

As already mentioned in the previous section, the present flow field is essentially three-dimensional, and so are the turbulent structures developing inside the channel. Sagaut (2000) presented a computation of this flow field by means of a Large Eddy Simulation. He detected the actual existence of horse-shoe type vortices developing from the upstream rib edge. The structures then detach from the rib surface and are convected by the main stream, causing the development of a 3D flow characterized by streamwise turbulent structures.

This experimental investigation is performed by means of a two-dimensional PIV technique. As a conseguence, the acquired flow fields are two dimensional, and this represents a constraint for the study of the CS in this type of flow. Along the "mean" flow symmetry plane the three-dimensional character of the flow field should be less marked than in any other flow plane. For this reason, the CS eduction was applied on the "mean" flow symmetry plane only.

### 4.1 The Eduction Method

Several methods to educe CS have been developed in the past years. Each of them is based on different considerations of intuitive topological or energetic nature. A wide overview on the available eduction methods was recently presented by Bonnet et al. (1998).

In the present work the Continuous Wavelet Transform (CWT) analysis is applied to study the coherence of the flow. This paper does not intend to present an exhaustive discussion about wavelet transforms and their applications to turbulence. A very clear and complete description can be found in literature (Lawalle, 1998; Farge, 1992). The present objectives are to motivate, by introducing only the basic concepts, the application of wavelets to the CS eduction and to briefly describe the used eduction algorithm.

In the development of an eduction method, the first step is to define the CS prototype. Many definitions are proposed in the literature. Combining the concepts elaborated by Hussain (1986) and Farge (1992), the CS prototype is defined as "an instantaneously and locally space correlated condensation of the vorticity field". In this way, the priority is given to the most energetic structures. The following step consists in the identification of the appropriate indicator function for the presence of such a singularity in the flow. The wavelet transforms allow to decompose a given signal into a basis of functions that have a bounded frequency content and are, in addition, localized in space. It is usually said that the wavelet transform has the property to be localized in space and scale (Farge, 1992) and therefore, it seems natural to study the behavior of local events (coherent structures) carrying a finite energy (vorticity peak associated to the structure) by using test functions which are themselves localized in space and of finite dimensions.

The code used to apply the CWT to the recorded two-dimensional PIV flow fields has been developed at VKI by Schram and Riethmuller (2001) for a laminar flow and Schram et al. (2002) for a turbulent flow.

The chosen indicator function for the presence of CS is the CWT of the enstrophy (vorticity squared) field. The latter, has been selected instead of the vorticity to give a stronger priority to the energetic structures The enstrophy is computed directly from the PIV flow fields after spatial filtering (with a 3x3 window of data points) of the data to eliminate the measurement noise and to make the code more robust.

The chosen mother wavelet type (the wavelet used to generate the wavelet family to cover the full range of size and energy of the structures actually present in the analyzed flow field) is the Marr wavelet. It was chosen by the authors of the code because it is well localized in space and because of its similar shape with the enstrophy distribution in the core of the Oseen vortex. The latter is taken as a model vortex for the calibration of the code. This calibration is indeed needed to determine the relation existing between the size of the detected vortex core and the size of the wavelet matching the detected structure.

The results extracted form the CWT are checked against three thresholds acting on :

i) the wavelet coefficients directly linked to the energy carried by the CS,

ii) the isotropy of the structure by comparing the CWT coefficients with the calibration done on the Oseen synthetic vortex,

iii) the sign of the second eigenvalue of the tensor $S^2 + \Omega^2$, where $S^2$ and $\Omega^2$ are the symmetric and anti-symmetric part of the velocity gradient tensor.

The last threshold is based on the Jeong and Hussain criterion (1995) to detect the presence of swirling motion associated to the actual presence of a vortex. Indeed, the last two checks were implemented to separate the vorticity associated to real swirling motion from the vorticity due to shear layers. It is worth mentioning that the last threshold requires the flow to be planar, otherwise the calculation of the eigenvalue would require the component of the velocity

gradient tensor which is not measurable by means of 2D PIV. The third threshold can therefore be switched off if the investigated flow presents an significant 3D character.

### 4.2 Results

The vortices educed from the 300 instantaneous flow fields of the plane 1xy are superimposed in Fig. 16 on the Reynolds stresses contour plot. The red circles and the black crosses indicate the center of the vortices with negative (clockwise rotating) and positive (anti-clockwise rotating) vorticity respectively. For sake of clarity, only the vortices characterized by a ratio (Core_size/h) larger than 0.11 are shown in this figure. The huge majority of these structures emanates from the shear layer, while a small part comes from upstream, being evidently generated in the first three inter-rib spacings. Two reasons explain the dissymmetry between the number of detected vortices with negative and positive vorticity. Most of the structures come from the breakdown of the shear layer with negative vorticity in this investigation. Furthermore, the structures with positive vorticity have been observed to be weaker, as will be shown later. Those structures could therefore fall below the thresholds set for the processing.

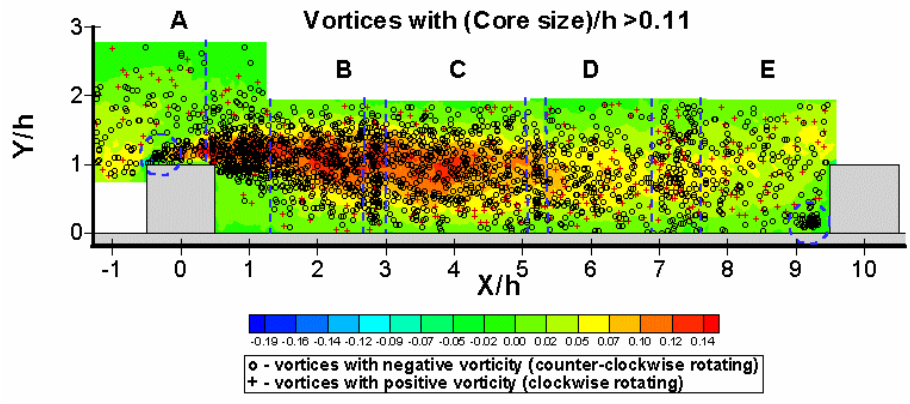


**Fig. 16 : Educed structures in the symmetry plane 1xy**

Above the rib and in its bottom front corner, one distinguishes 2 accumulations of structures (marked by the two circles in Fig. 16), which correspond, in the "mean" flow, to the separation bubbles $V_2$ and $V_3$. From the results of the wavelet analysis one can therefore suppose that those structures are not only characteristics of the "mean" flow but are really present in the instantaneous flow field. The structures detected in the averaged flow field are evidently the statistical representation of the real instantaneous flow patterns detected by the wavelet analysis. The same remark can evidently not be stated for the "mean" large separation bubble behind the rib, where many small, widely dispersed structures are found. In the downstream bottom corner of the rib no vortices are detected to confirm the instantaneous nature of the structure there found in the "mean" flow. This is most probably due to the imposed threshold value on the vorticity, too small to allow their detection. Three additional zones characterized by an accumulation of vortices are marked by vertical dashed lines in Fig. 16. This behavior is only due to the overlapping of the measurement zones and does not have any physical meaning.

A statistical analysis of these results provides the evolution of the "mean" vortex characteristics and the determination of a most likely structure (or "preferred mode") in the flow field. The statistics are based on the complete population of educed structures to ensure the convergence. Plane 1xy is divided in 5 different zones, corresponding to the recording areas of the measurements (zones A to E, Fig. 16). A bad convergence of the statistics is observed in zone A, in which the shear layer is generated. Therefore, small flow portions, characterized by strong shear, are present in the instantaneous velocity fields. It was very difficult to reject the shear layer vorticity with the set of previously defined thresholds that were properly working for the 4 other zones. More severe thresholds could be used, especially on the isotropy of the structure and on $\lambda_2$, but this would lead to miss part of the vortices in the downstream zones. Therefore, the results on zone A are not included in the statistical analysis, to preserve the quality of the conclusions drawn from the statistics.

The evolution of the total number of educed structures, their mean core size, mean vorticity and mean circulation within plane 1xy are presented in Fig. 17. The core size and the vorticity are normalized with respect to the rib height (30 mm) and the bulk velocity (6.2 m/s).

The trend in the evolution of the CS detected in plane 1xy is clear from Fig. 17. The total number of educed structures is reduced by 65% when moving downstream, while the absolute values of the "mean" circulation and of the vorticity are reduced by almost 50%. A slight increase of the core size (4%) is noticed. The decrease of vorticity and circulation is associated with the dissipation of energy taking place in the turbulent structures. The increase in core size is of the same order of magnitude as the error made in the evaluation of the averages. To verify this, the averaging process was applied over the flow region where zone D and E overlap ($7.0<X/h<7.7$). The statistics did not seem to be

completely converge, since a small variance in the used number of samples (11%) leads to differences in the averaged values. Therefore, a physical meaning can not definitely be given to the mean core size evolution.

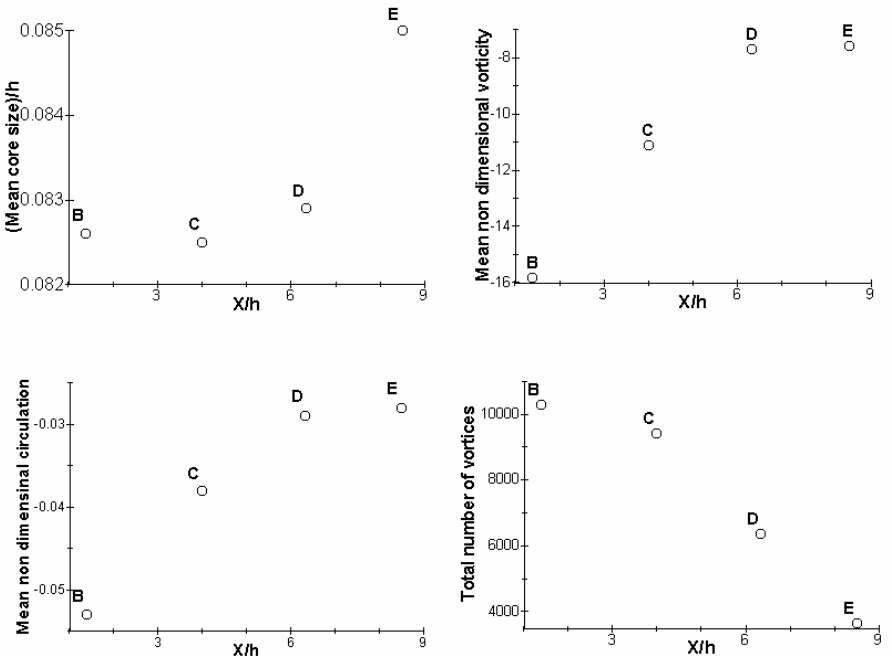


**Fig. 17 : Total number of educed structures (top left), mean core size (top right), mean circulation (bottom left) and mean vorticity (bottom right) within plane 1xy**

The statistical distributions of core size, vorticity and circulation for zone B are reported in Fig. 18. The strongly dissymmetric distributions of vorticity and circulation, confirm the predominance of clockwise structures with respect to the anti-clockwise ones. Moreover, the distributions are very narrow and suggest the existence of a preferential mode in the present flow field. To confirm this, one has to verify if the structures that give the peak in size, are the same than those which give the peak in vorticity or circulation. The joint probability distributions of size-vorticity, vorticity-circulation and circulation-size were computed for the complete set of data. One of these results is show in Fig. 19 (the others are similar), confirming the presence of a single peak in each probability distribution map. This confirms the presence of a preferred mode inside the CS population around the values:

(Core_size)/h = 0.073; Circulation peak = 0.045; Vorticity peak = 19

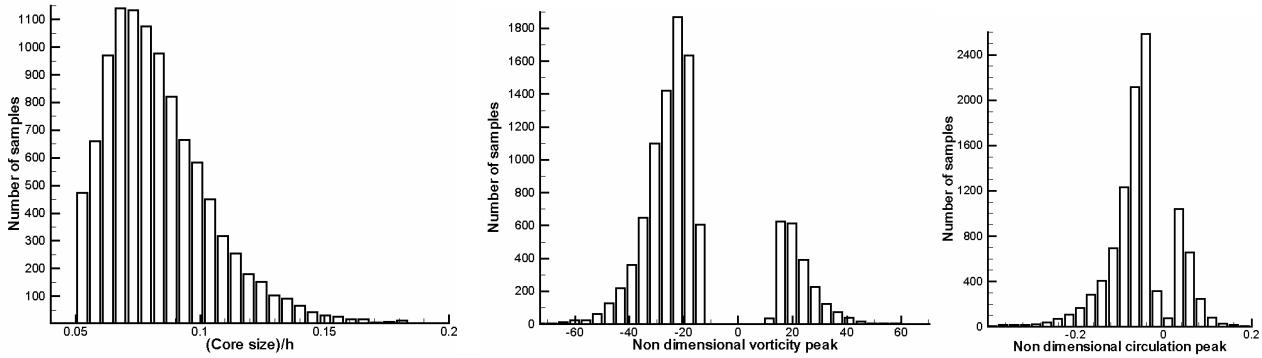


**Fig. 18 : Statistical distributions of core size, vorticity and circulation of the educed structures in zone B of plane 1xy**

The same conclusions are obtained by analyzing the data in the 3 other measurement regions (C, D and E) but not presented here because of lack of space. A sub-class of vortices centered around that mode ($0.068<(\text{Core\_size})/h<0.078$, $13<\text{Vorticity peak}<25$) was ensemble averaged over the four zones, gathering 2960 samples (or "phase aligned vortices") (887, 1006, 693 and 374 samples in zone B, C, D and E respectively). The resulting averaged vorticity pattern and its RMS are represented in Fig. 20. The isotropy of the "most likely" vortex is well respected. The standard deviation of the phase-aligned vorticity is limited to 20% in the core and to 35% over twice this region in spite of the relatively large number of phase-aligned structures that were averaged.

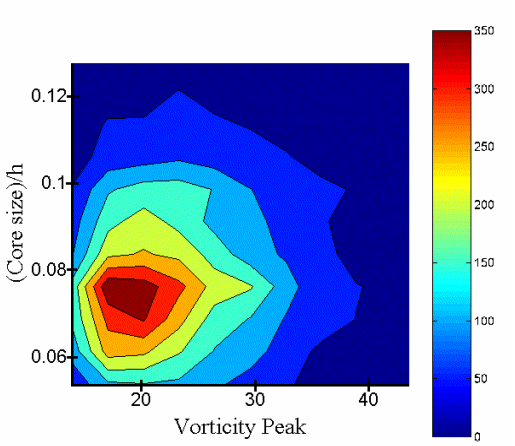


**Fig. 19 : Combined statistical distribution of the core size and vorticity peak in zone B of plane 1xy**

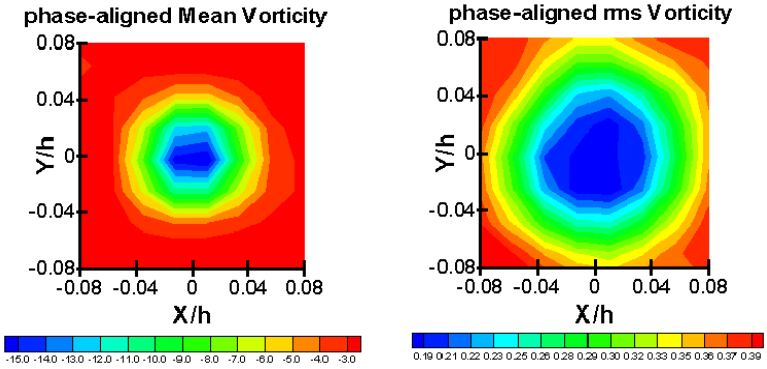


**Fig. 20 :Coherent vorticity pattern and its rms (normalized by (Mean vorticity)$_{max}$) associated to the preferred mode in zone B of plane 1xy**

## 5. CONCLUSIONS

The velocity field inside a turbine blade coolant passage equipped with high blockage turbulence promoters was investigated in great detail by means of Particle Image Velocimetry. The measurements were conducted on a scaled up model working at correct geometrical and kinematic similarity conditions. The time–averaged flow field allows an exhaustive description of the three-dimensional mean flow topology. The turbulent phenomena are found to be highly anisotropic, showing streamwise fluctuations 2 times higher than in the vertical or spanwise directions. The comparison with the available wall heat transfer data shows a correlation between the high level of fluctuations and heat transfer. In particular, along the ribbed wall, the velocity fluctuations normal to the wall seem to be the driving parameter in the development of the heat transfer field. These observations should provide some useful guidelines in the selection of the appropriate turbulence model.

The PIV data within the flow symmetry plane are further post-processed by means of a Continuous Wavelet Transform procedure for the eduction of the coherent structures. On one side, the resolution achieved by PIV allows the identification of the most energetic structures in the flow field. On the other side, the selectivity in space and scale of the CWT permits to detect and characterize in dimensions and intensity the singularities of the flow field, namely the CS. The evolution of the structures mean characteristics is well put in evidence over the full inter-rib space. In particular two separated flow regions, on top and upstream of the obstacle, detected in the time averaged flow field, also show an instantaneous character.

Finally, a preferred mode based on the core diameter, vorticity peak and circulation of the educed CS is identified and its coherent vorticity computed.

## REFERENCES

Bonnet, J. P.; Delville, J.; Glauser, M. N.; Antonia, R. A.; Bisset, D. K.; Cole, D. R.; Fiedler, H. E.; Garem, J. H.; Hilber, D.; Jeong, J., Kevlahan, N. K. R.; Ukeiley, L. S.; Vincendeau, E. (1998): “Collaborative testing of eddy structure identification methods in free turbulent shear flow”, Experiments in Fluids, Vol. 25, pp 197-225.

Çakan, M. (2000): “Aero-thermal investigation of fixed rib-roughened cooling passages”, Ph.D. Thesis, Université Catholique de Louvain, von Karman Institute for Fluid Dynamics, June 2000.

Casarsa, L.; Çakan, M.; Arts, T. (2002): “Characterization of the velocity and heat transfer fields in an internal cooling channel with high blockage ratio”, GT-2002-30207, ASME TURBO EXPO 2002, Amsterdam, June 2002.

Chanteloup, D.; Bolcs, A. (2001): “PIV investigation of the flow characteristics in 2-leg internal coolant passage of gas turbine airfoils”, 4th European Conference on Turbomachinery, Florence, Italy.

Cramer, H. (1995): “The element of probability theory and some of its applications”, Wiley & Sons, New York.

Durbin; P.A. (1993): “Application of a near wall turbulence model to boundary layers and heat transfer”, Int. J. Heat and Fluid Flow, Vol. 14, pp 316-323

Farge, M. (1992): “Wavelet transforms and their applications to turbulence”, Ann. Rev. of Fluid Mechanics, Vol. 24

Han, J. C. (1998): “Heat transfer and friction characteristics in rectangular channels with rib turbulators”, ASME J. of Heat Transfer, Vol. 110, No. 2, pp 321-328.

Han, J. C.; Zhang, Y. M.; Lee, C. P. (1992): ”Influence of surface heat flux ratio on heat transfer augmentation in square channels with parallel, crossed and V-shaped angled ribs”, ASME J. of Turbomachinery, Vol. 114, pp 872-880.

Hermanson, K.; Parneix, S.; Von Wolfersdorf, J.; Semmler, K. (2001): “Prediction of pressure loss and heat transfer in internal cooling passages”, Heat Transfer in Gas Turbine Systems, Ed. R. Goldstein, New York Academy Sciences, Vol. 934.

Hussain, F. (1986): “Coherent Structure and Turbulence”, J. of Fluid Mechanics, Vol. 173; pp 303-356.

Jeong, J.; Hussain, F. (1995): “On the identification of a vortex”, J. of Fluid Mechanics, Vol. 285, pp 69-94

Lawalle, J. (1998): “Application of continuous wavelet to data analysis”, VKI Lecture Series 1998-06, von Karman Institute for Fluid Dynamics, Belgium.

Liou, T. M.; Hwang, J. J.; Chen, S. H. (1993): “Simulation and measurement of enhanced turbulent heat transfer in a channel with periodic ribs on one principal wall”, Int. J. of Heat and Mass Transfer, Vol. 36, pp 507-517.

Rau, G. (1998): “Einfluss der Rippenanordnung auf das Strömungsfeld und den Wärmeübergang in einem Kühlkanal mit quadratischem Querschnitt”, Ph.D. Thesis, Technischen Universität Darmstadt, Germany.

Rau, G.; Moeller, D.; Çakan, M.; Arts, T. (1998): “The effect of periodic ribs on the local aerodynamic and heat transfer performance of a straight cooling channel”, ASME J. of Turbomachinery, Vol 120, pp 368-375.

Riethmuller, M. L.; Lourenco, L. (1981): “Measurements in particulate two phase flow”, VKI Lecture Series 1981-3, von Karman Institute for Fluid Dynamics, Belgium.

Rigby, D.L. (2000): “Numerical simulation of non rotating and rotating coolant channels flow fields”, VKI Lecture series 2000-03, von Karman Institute for Fluid Dynamics, Belgium.

Sagaut ; P. (2000): “Application of LES and DNS to internal cooling channels”, VKI Lecture Series 2002-03, von Karman Institute for Fluid Dynamics, Belgium.

Scarano, F.; Riethmuller, M.L. (1999): “Iterative multigrid approach in PIV image processing with discrete window offset”, Experiments in Fluids, Vol. 26, pp 513-523.

Schabacker, J.; Boelcs, A.; Johnson, B. V. (1999): “PIV investigation of the flow characteristics in an internal coolant passage with 45° rib arrangement”, International Gas Turbine & Aeroengine Congress & Exhibition. Indianapolis, Indiana, USA, 99-GT-120.

Schram, C.; Riethmuller, M.L. (2001): “Vortex ring evolution in an impulsively started jet using digital particle image velocimetry and continuous wavelet analysis”, Measurement Science and Technology, Vol. 12, pp 1413-1421.

Schram, C.; Rambaud, P.; Riethmuller, M.L. (2002):"Wavelet based coherent structure eduction from a backward facing step flow investigated with particle image velocimetry". Submitted to Experiments in Fluid.

Taslim, M. E.; Wadsworth, C. M. (1997): "An experimental investigation of the rib surface averaged heat transfer coefficient in a rib roughened square passage", ASME J. of Turbomachinery, Vol. 119, pp 381-389.